Mahaarachchi, Dhammika P. and Mahendran, Mahen (2009) *A strain criterion for pull-through failures in crest-fixed steel claddings.* Engineering Structures, 31(2). pp. 498-506.

A Strain Criterion for Pull-through Failures in Crest-fixed Steel Claddings

By Dhammika Mahaarachchi[1] and Mahen Mahendran[2]

Abstract

Crest-fixed steel claddings made of thin, high strength steel often suffer from local pull-through failures at their screw connections during high wind events such as storms and hurricanes. Adequate design provisions are not available for these cladding systems except for the expensive testing provisions. Since the local pull-through failures in the less ductile steel claddings are initiated by transverse splitting at the fastener holes, numerical studies have not been able to determine the pull-through failure loads. Numerical studies could be used if a reliable splitting criterion is available. Therefore a series of two-span cladding and small scale tests was conducted on a range of crest-fixed steel cladding systems under simulated wind uplift loads. The strains in the sheeting around the critical central support screw fastener holes were measured until the pull-through failure occurred. This paper presents the details of the experimental investigation and the results including a strain criterion for the local pull-through failures in crest-fixed steel claddings.

Keywords: Crest-fixed steel cladding systems, Screwed connections, Local pull-through failures, Wind uplift loads, Experiments, Strain criterion

[1] – PhD Researcher

[2] –Professor of Structural Engineering

1. INTRODUCTION

In Australia and its neighbouring countries, trapezoidal and corrugated steel roof claddings made of thin (0.42 mm base metal thickness), high strength steel G550 (minimum yield stress 550 MPa) are commonly used in the building industry. They are always crest-fixed when used as roof cladding as shown in Figure 1. The connection between roof sheeting and battens/purlins is often the weakest link in the structural system when subjected to wind uplift loading. The loss of roofing results in severe damage to the entire building and its contents. This situation is continuing because of the lower priority given to the design of roof and wall cladding systems.

Field and laboratory investigations and past researches (Mahendran, 1994, Beck and Stevens, 1979, Xu and Reardon, 1993) have shown that loss of steel roofs has often occurred due to local failures of their screwed connections. The presence of large stress concentrations around the fastener holes under wind uplift loading is attributed to the local pull-through or pull-over failures at screwed connections in which the roof sheeting is pulled through or pulled over the fastener heads (see Figure 2a). These failures are initiated by a transverse split at the screw fastener hole (Mahendran, 1990a,b, Mahendran and Tang, 1999). For some steel roofing, a local dimpling failure occurs without any transverse splitting/fracture (see Figure 2b). In this case the disengagement of sheeting does not occur and it is a preferred failure mode. Past research has shown that the stress/strain patterns around the fastener hole are very complicated. However, it is considered that there must be a unique strain criterion for the transverse split caused pull-through failures. This paper is therefore aimed at determining this criterion, which can be used in the numerical modelling of crest-fixed steel claddings.

Currently, the Australian cold-formed steel structures standard AS/NZS 4600 (SA, 2005) gives the following formula for the capacity of screwed connections in tension (F_{ov}).

$$F_{ov} = 1.5\, t\, d_w\, f_u \qquad (1)$$

where t = thickness of steel cladding material

d_w = larger value of the screw head or the washer diameter ≤12.5 mm

f_u = ultimate tensile strength of steel

However, its accuracy for the pull-through strength of crest-fixed claddings is questionable, and thus cladding manufacturers rely on an expensive testing process. Recently, Mahendran and Tang (1999) have developed a design formula for the pull-through strength of crest-fixed steel claddings.

$$F_{ov} = c\, d_w^{\alpha}\, t^{\beta}\, f_u^{\chi} \qquad (2)$$

where c = 0.22,0.23, α = 0.4,0.2, β = 2.2,1.7, χ = 0.4,0.4 for the standard trapezoidal claddings Type A (with wide pans) and Type B (with closely spaced ribs) shown in Figure 1(a), respectively, while others have been defined in Equation (1) above.

However their research was mainly based on small-scale tests, and has not resolved the critical issue of splitting at the screw holes.

Since the local pull-through failures in the less ductile G550 steel claddings are initiated by transverse splitting at the fastener hole, Tang (1998) found that the finite element analyses could not predict the failure loads as elastic- perfect plastic material behaviour with infinite ductility is assumed without any allowance for splitting. Numerical studies could be used only if a reliable splitting criterion is available. Therefore a series of full-

scale two-span cladding tests was conducted on a range of crest-fixed steel cladding systems under simulated wind uplift loads. The strains in the sheeting around the critical screw fastener hole were measured until the pull-through failure occurred. The results were then used to develop a strain criterion. The failure loads were also used to verify the design formula (Equation 2) developed recently from small-scale tests. This paper presents the details of this experimental investigation and the results.

2. EXPERIMENTAL METHOD

Analyses of a multi-span roofing assembly show that the critical second support from the eaves or ridge of the roof is adequately represented by the central support of a two-span roofing assembly. Therefore in this study a two-span roofing assembly with simply supported ends was tested under a wind uplift pressure loading (see Figure 3a). In order to accurately simulate a uniform wind uplift pressure, an air box measuring 1800 mm wide by 4200 mm long by 300 mm deep was used (Figure 3b). The test roofing assembly was set-up up side down in the air-box, which was then sealed with 4.5 μm polythene sheets. The uniform wind uplift pressure was simulated by extracting the air from the air box using a vacuum pump. Most of the test roofing assemblies were 800 mm wide (one sheet wide) × 1000-2300 mm long as their span was varied from 425 to 1100 mm (Figure 3c). The gaps on both sides of the roofing assembly were filled with polystyrene foam.

The trapezoidal Type A (Figure 1) roofing sheets were fastened at every crest whereas trapezoidal Type B and corrugated roofing sheets were fastened at alternate crests as recommended by the manufacturers. In order to investigate the splitting mechanism in a variety of roofing profiles and to determine the effect of profile geometry on splitting

criterion, many non-standard Type A roofing sheets were made in the university workshop and were used in the tests with a shorter span of 425 mm and also in some small scale tests (see Tables 1 and 2). The No.14-10x50 mm Type 17 self-drilling screws with neoprene washers were used to secure the test sheet to the timber supports. The No.14 screws have head and shaft diameters of 14.5 mm and 5.1 mm, respectively and the 2 mm thick neoprene washers have outside and inside diameters of 11 mm and 5 mm, respectively. All the screws were centred at the crests, set perpendicular to the plane of the sheet and tightened until the neoprene washers were just prevented from rotating to avoid over-tightened or loose screws.

The load per fastener at the central support is an important parameter controlling the pull-through failures (Mahendran, 1994). Therefore two 5 kN load cells were used to measure the loads in two of the central support fasteners. For this purpose the crests of roofing and the central support purlins were predrilled for the insertion of specially made screws. These special screws had the same No.14-10 screw heads, but had a longer shaft (300 mm). The 5 kN load cells were inserted within the longer shaft and tightened with end plates (see Figure 4). In addition to the measurement of individual fastener loads at the central support, the reaction forces at the ends of central and end support purlins were also measured using four 30 kN load cells (see Figure 3a). The latter measurements enabled the determination of the average load per fastener at the central support. The pressure in the air box was monitored by a pressure gauge that had been calibrated with a manometer. It was then used to calculate the nominal load per fastener at the central support using a simple formula. Deflections of the steel claddings were measured using five displacement transducers at important locations such as the central support and midspan crests and pans (see Figure 3).

Eight 2 mm strain gauges were used in each test to determine the strains in the roofing in the vicinity of central support fasteners. Since the principal strain directions were unknown, three arm 45-degree strain gauge rosettes were placed near the two predrilled fastener holes (about 1 mm from the edge of the hole) where the individual load cells were used. The strain gauges were placed in the longitudinal (L) and transverse (T) directions in corresponding positions on both the top and bottom surfaces of the sheeting in order to determine both membrane and flexural strain components (see Figure 4).

In the preliminary tests, two roofing sheets were used as specified in AS 4040.2 (SA, 1992). The use of two sheets gave a specimen width of 1400/1350 mm for Types A and B trapezoidal claddings compared with 820/770 mm for single sheets. The number of central support fasteners was 5 and 8, respectively.

In a number of two-span cladding tests, the exact failure strains at the moment of splitting could not be recorded because the rate of recording (at 15 sec intervals) of the computer system used was inadequate to handle the rapid variation of strains at failure. Therefore a series of small-scale tests using the method recommended by Mahendran (1994) was conducted as shown in Figure 5. In this method, the tensile load in the specially made screw fastener with a long shaft was increased until the sheeting split using a simple hand tightening method. Although the small-scale tests may not produce accurate pull-through failure loads, their strain results can be used in the determination of a suitable criterion for splitting. Therefore the strain results from the small-scale tests were used in the determination of suitable strain criteria (Table 2).

3. DISCUSSION OF EXPERIMENTAL RESULTS

The results from single and two-sheet roofing assemblies were approximately the same as shown in Figure 6. This observation is an important and useful result. It meant that the structural continuity was absent in the lateral direction because of the presence of longitudinal laps. The single sheet roofing assembly provided a more uniform load distribution among the fasteners, and eliminated the additional stiffening problem caused by the lap and simplified the test procedure. Therefore a single sheet roofing assembly was used in most of the tests (see Figure 3).

3.1 Load per fastener

The fastener reaction was the largest at the central support and therefore the local pull-through failures (dimpling or splitting) occurred only at the central support screw fasteners (see Figures 2(a) and (b)). Tests showed that the failure is governed by the magnitude of the central support load per fastener. The measured individual fastener loads were compared with predictions from simple equations 3 and 4 in Figures 7(a) and (b). Equation 3 calculates the load per fastener from the measured uniform pressure based on a two-span beam behaviour whereas Equation 4 is based on a single span beam behaviour.

$$\text{Load per fastener} = 1.25 \times \text{wind pressure} \times \text{span} \times \text{distance between fasteners} \quad (3)$$

$$\text{Load per fastener} = \text{wind pressure} \times \text{span} \times \text{distance between fasteners} \quad (4)$$

The average load per fastener was also calculated by dividing the measured central support reaction by n and n-1, where n is the total number of fasteners at the central

support (for single sheet roofing assembly, n is 5). This is also plotted in Figures 7(a) and (b). Table 1 gives the failure loads per fastener from the full scale tests.

The load per fastener value obtained from Equation 3 was generally greater than the measured loads. It appeared that the coefficient of 1.25 in the simple formula, which is based on linear theory assuming elastic material and no cross-sectional distortion (Mahendran 1994), has to be revised depending on the roofing profile and level of loading. The measured fastener loads are also between the average loads per fastener, calculated by dividing the central support reaction by 5 and 4. Therefore the assumption made by the previous researches that the support reaction is distributed uniformly among the fasteners is questionable. The use of simple Equations 3 and 4 to determine the critical central support fastener load from the measured pressure is also not accurate. Therefore in this paper the measured loads per fastener obtained directly from the individual load cells were used.

The actual fastener load measured using individual load cells appear to be less than the average fastener load (see Figures 7(a) and (b)). The average fastener load was calculated assuming that the fastener reaction is proportional to the tributary area under wind uplift load. This assumption will not be true if there is a stiffness variation across the steel cladding assembly. In particular, the cladding assembly used in this investigation had two unsupported edges which led to weaker end pans during the experiments and thus smaller than the average fastener load.

As seen in Figures 7 (a) and (b), the load per fastener was approximately linear with upward pressure for loads up to about 600 N. At loads closer to failure, the central support load per fastener suddenly dropped in Type B roofing assembly and then

increased further while it was constant and then increased for Type A roofing assembly. This is because the roofing assembly does not behave as a two span beam after local yielding. Instead it behaves as a single span beam. This can be seen in Figures 7(a) and (b), where the measured fastener loads agree well with Equation 4 predictions after yielding or local failure. Therefore it is reasonable to assume post-failure stage roofing assembly as a single span beam, which implies that in post-local failure deformations, sheeting cross section at the central support sustained only small global bending moments. The above outcomes and observations are useful to researchers and engineers who undertake wind uplift pressure tests of various profiled steel cladding assemblies (two-span) in order to develop design wind pressure tables.

Pull-through failure loads were calculated by using Equation 1 based on AS/NZS 4600 (SA, 2005). In these calculations, 75% of the specified minimum strength of G550 steel was used since the steel roof cladding thickness was less than 0.6 mm. The results (Table 1) show that this design formula is incapable of predicting the failure strength of crest-fixed steel cladding systems considered in this investigation. The design formula (Equation 2) recommended by Mahendran and Tang (1999) appears to be more suitable (Table 1) than the current design formula for the pull-through strength of crest-fixed cladding systems, but is also inadequate in some cases. This inadequacy is mostly observed with non-standard profiles that were made in the transverse direction. This is due to the fact that Equation 2 was developed based on tests of standard profiles made in the longitudinal direction.

3.2 Load-deflection Behaviour

Trapezoidal roofing Type B

Typical load-deflection curves for this roofing (1100 mm span) are given in Figure 8. They exhibit four stages of behaviour. During the first stage, the behaviour was linear elastic and can be predicted using simple engineering theories. This situation prevails until the fastener reaction reaches around 600 N. With further increase in load, large cross-sectional distortions were observed followed by localised deformation and yielding around the fastener holes. These dimples extended further in the longitudinal direction of the sheeting with load increase in the second stage. When the load per fastener reached about 1000 N, large local plastic deformations occurred causing further cross-sectional distortion without any load increase. Side plates of the ribs at central fastener buckled with the crest dimpling beyond the edge of the ribs. Although the occurrence of local plastic deformations around the central support fastener could be considered as an initial failure (Mahendran, 1994), the sheet deformed further with the load increasing steadily again during Stage 4. This could be explained by the fact that once side plates flattened, the area around the central fasteners was subject to a membrane behaviour while surrounding sheeting restricted that through large bending strains. This situation continued until the crests and valleys of mid span cross-section began to deform severely that led global plastic mechanisms to form at each midspan when valleys failed by buckling. Soon after this, a pull-through failure occurred in the central support fasteners.

Trapezoidal roofing Type A

The load-deflection curves for this roofing of 900 mm span with three stages of loading are presented in Figure 9. As for the Type B roofing the uplift load caused severe cross

sectional distortion since the screwed ribs are separated by a wide pan. For fastener loads up to 600 N the behaviour of roofing was elastic. With increasing loads, the crests slightly dimpled, but not as severe as in Type B roofing. This was followed by a membrane action of the region and plastic dimples became larger. This situation was almost similar for all the spans, but for spans less than 1000 mm, local plastic failure of side plates of ribs can be observed when central support fastener reaction reached around 1200 N and it led to a transverse split followed by screw head pulling through the sheeting. For the larger span of 1100 mm, the behaviour and failure were similar to that of Type B roofing. But it did not have the reserve capacity as for Type B roofing since mid span valleys buckled at a smaller load compared with Type B roofing.

Corrugated roofing

The behaviour of corrugated roofing was similar to that of trapezoidal Type B roofing. However, the local failure load was considerably smaller than that of trapezoidal Type B roofing. The failure was always governed by local dimpling of crest without any transverse splitting or fracture. Detailed studies into the behaviour of corrugated cladding have already been undertaken by other researchers (Mahendran, 1990a,b, Xu and Teng, 1994). Therefore this paper does not describe in detail the behaviour of corrugated cladding systems.

It was found that the different span assemblies gave approximately the same fastener load at failure for both trapezoidal Type A and Type B claddings as the failure was localised at the central support fastener holes. Therefore fastener failure load can be used in the design of cladding assemblies with varying spans. These observations are

similar to those observed by other researchers (Mahendran, 1990a,b, 1994 and Xu and Teng, 1994).

When larger washers were used, the local and overall deformations were reduced while the fastener failure load was increased. Although some local dimpling deformations occurred around the screw fasteners at the central support, splitting/fracture was not observed. Experiments also showed that increasing the cladding thickness significantly enhanced the ultimate failure load. The fastener failure load of the trapezoidal Type B cladding with 0.42 mm base metal thickness (bmt) was 1063 N (6.8 kPa) while it was 1300 N (8.74 kPa) for the 0.48 mm bmt cladding.

3.3 Development of a Suitable Fracture/Splitting Criterion

The microscopic investigation showed that there were no cracks or crack-like defects along the edge of the fastener hole (due to drilling or other reasons) before any load was applied. Therefore it is very important to investigate how transverse split/crack (or fracture) was initiated in the crack-free steel sheeting. Tensile testing of G550 steel coupons showed that it has very little strain hardening and the failure strain is only about 2%. This provides some explanation for the premature transverse splitting at the fastener holes. However, the 2% failure strain was obtained for steel in pure tension (membrane only). Its applicability to steel sheeting around the fastener hole subject to combined membrane and bending actions is questionable. Although the same steel was used, some cladding systems suffered from local pull-through failures with transverse splitting (most of Type A sheeting) while there was no splitting in other claddings. This observation indicates that there are other reasons for the splitting phenomenon.

In the local pull-through failures observed at the central support fastener holes, there was considerable plastic flow (local dimples) and extensive permanent deformation before fracture and the failure strains were quiet large compared with the yield strain. A transverse splitting/fracture occurred in the less ductile sheeting within the highly strained regions of central support fastener holes. Hence the pull-through failure can be classified as a ductile plastic failure (Atkins and Mai, 1985). However, a proper theoretical basis of combined flow and fracture is not yet fully developed for such fractures. In such cases, Atkins and Mai (1985, 1987) recommends the use of experimental data concerning plastic strains local to the fracture sites to establish a criterion for crack initiation in ductile fractures. Crack initiation (splitting) occurs by combined in-plane membrane and bending strains in the fastener hole region and can be defined easily in terms of critical strains because of the highly localised deformation region. Therefore the strain results obtained from the cladding tests were used to develop a suitable splitting/fracture criterion for local pull-through failures of thin, profiled steel claddings.

Figures 10 (a) and (b) present the typical percentage strain variations on the longitudinal and transverse sides of the central support fastener hole with increasing uplift pressure. The membrane strain was obtained by averaging the top and bottom surface strains while the flexural strain was obtained by dividing the difference in the surface strains by two. The high membrane and flexural strains in the longitudinal direction on the transverse side of the fastener hole indicate why fracture occurs on the transverse side. For smaller uplift pressures, the longitudinal membrane strain on the transverse side was compressive due to the global bending of sheeting as a two-span beam. With increasing uplift pressures, this situation is modified and the longitudinal membrane strain becomes tensile due to the local deformations around the fastener hole (see Figure

10a). The failure strains including the membrane and flexural components on the transverse side of fastener hole were analysed and the results are listed in Table 2. They are also plotted in Figures 11 to 15.

The sheeting around the fastener hole is subjected to both global bending effects, and local effects due to fastener reaction. Therefore the crest of sheeting around the fastener hole is subjected to a local bending action and a membrane compression force due to global bending. The presence of both membrane and flexural strain components around the fastener hole makes the current problem different from other works of penetration and perforation of steel plates (Muscat-Fenech and Atkins, 1998), and more complicated.

The magnitude of the limiting failure strain of sheet metal depends both on the loading, the ratio of the principal strains and the following material properties (Marciniak and Kuczynski, 1967): the initial in-homogeneity of the sheet, the coefficient of anisotropy and the strain hardening curve. Since all the experiments were conducted for G550 steel and the manufacturing process is the same, effects of inhomogeneity and anisotropy can be neglected. Tensile tests showed that G550 steel has no strain hardening. Therefore the influence of material properties on the limiting strains is considered small.

Marciniak and Kuczynski (1967) pointed out that the most probable direction of fracture is perpendicular to the direction of the major principal strain. The relationships between the principal strains and longitudinal and transverse membrane strains for the trapezoidal steel claddings are therefore plotted in Figures 11 (a) and (b). These figures show that the major and minor principal strains are in the direction of longitudinal and transverse directions, respectively. Fracture/splitting at the fastener hole was always in

the transverse direction or perpendicular to the longitudinal or major principal strain direction and thus agree closely with Marciniak and Kuczynski's (1967) observations.

From Figures 11 (a) and (b), it is clear why fracture always occurs in the transverse direction of the steel cladding. Initiation of fracture occurs after the sheet around the fastener is deformed and stretched over the screw head. This situation can be described by the Fracture Forming Limit Diagram (FFLD). Such diagrams give the in-plane strain pairs at which fracture occurs under different biaxial loading conditions. The FFLD can be obtained using Marciniak and Kuczynski's (1967) method. Figure 12 shows the FFLD of experimental maximum surface tensile strain at failure (e_{max}) versus the ratio of transverse (e_2) and longitudinal (e_1) membrane strains for all the tests that included both fracture and no-fracture. It is to be noted that e_{max} was based on the surface strain measurements and thus includes a combination of membrane and flexural strains. The G550 steel claddings had a tensile coupon failure strain of only 2% in the longitudinal direction, and for the same steel sheets, the tensile coupon failure strain was only about 0.8% in the transverse direction. Some non-standard profiled claddings were cold-formed using sheets in the transverse direction. Therefore the longitudinal failure strain of these specimens was considered as 0.8% (compared with 2% for other specimens). Therefore in Figure 12 e_{max} was normalised by using the corresponding tensile coupon failure strain (e_t).

The FFLD has been used successfully in the fracture problems of plates hit by an obstacle (Muscat-Fenech and Atkins, 1998). These diagrams give in-plane strain pairs at fracture for the plates subject to in-plane stretching. Steel sheeting around the fastener hole is subjected to a combination of in-plane stretching and bending, and is more complicated. Therefore Figure 12 gives mixed results of failure strains for fracture

and no-fracture cases. No attempts have been made so far to predict the failure strain using the FFLD in the case of combined membrane and flexural strains. Therefore attempts were made develop a relationship between flexural and membrane strains with the failure strains in a similar manner to FFLD. As shown in Figure 10 the longitudinal membrane tensile strains dominate the fracture/splitting. Figure 13 shows the relationship between the maximum surface tensile strain (e_{max}) and the longitudinal membrane strain (e_1) at the fastener hole.

Figure 13 data appears to show the difference between fracture and no-fracture cases. It is similar to the FFLD, but it may not stand alone as a failure criterion. The straight line is best fit line for the fracture cases and shows that fracture occurs when the longitudinal membrane strain is more than 62% of the maximum surface tensile strain. Data for the no-fracture case are located below this line. Therefore it can be concluded that for fracture to occur, the longitudinal membrane strain produced under the combined strain field should reach 62% of the maximum surface tensile strain at failure. This value is based on the best fit line for the fracture data, and a closer investigation shows that it, in fact, varies between 57% and 62%. Therefore allowing for the possible experimental errors, this value can be taken as 60%. The most important conclusion is that when fracture/transverse splitting occurs in profiled steel claddings where combined membrane and flexural strains dominate, the ratio of membrane strain in the longitudinal direction to maximum total (surface) tensile strain at failure must exceed 0.6.

The above criterion is a necessary condition, but is not sufficient. Therefore the maximum surface tensile strain at failure (e_{max})/ tensile coupon failure strain (e_t) was plotted with corresponding test number in Figure 14. Small scale tests also showed that

fracture initiated on the bottom side of the sheeting where the tensile strain was the largest. The recorded maximum tensile strain at fracture was found to be very close to the tensile coupon failure strain and therefore e_{max}/e_t is close to 1 in Figure 14 for most of the fracture cases than for no-fracture cases. The simple rule of Datsko (1966) states that the maximum strain that can be sustained without fracture is equal to the fracture strain in a tensile test. The observation in Figure 14 agrees well with this simple rule. It is seen that the strain ratio is smaller than 1 for some cases of fracture because in a number of two-span cladding tests, the exact failure strains at the point of fracture could not be recorded because the rate of recording (at 15 sec intervals) of the computer system used was inadequate to handle the rapid variation of strains at failure. In view of the complexity of the straining process near the fracture point in the steel claddings, this recorded value cannot be considered as enabling more than a general comparison of results. In some test results, the maximum surface tensile strains were greater than those in tensile coupon tests, i.e. e_{max}/e_t is greater than 1. Ghosh and Travis (1979) have also observed the failure strains to be greater than the tensile coupon failure strains in their research on piercing of thin diaphragms. Datsko's rule was developed for yielding and cracking in the material forming or rolling where pure membrane strains are involved and therefore it cannot be used alone in this problem where combined membrane and flexural strains are involved. The use of Datsko's rule alone in the finite element analyses of steel claddings was found to be inadequate in the prediction of splitting (Tang, 1998).

Based on Figures 13 and 14, it can be concluded that for the profiled steel claddings, the initiation of fracture/splitting takes place when the membrane tensile strain in the longitudinal direction/maximum surface tensile strain ratio exceeds about 0.6 and the maximum surface tensile strain exceeds the tensile failure strain observed in a tensile

test. This is a significant observation than what has previously been assumed in past researches. The accuracy of the proposed strain criteria is also shown reasonably well in Figure 15, which is a plot of e_1/e_{max} versus e_{max}/e_t. Due to the limitations in recording failure strains accurately during the test, all the data points do not confirm to the proposed strain criteria. However, in general, fracture and no-fracture cases validate the proposed strain criteria adequately. For example, most cases of no-fracture data points had either the value of e_1/e_{max} well below 0.60 or that of e_{max}/e_t well below 1.0 (see Figure 15).

In summary, the series of small scale and large scale steel cladding tests have shown that transverse splitting/fracture of high strength steel claddings occurred at the edge of the screw fastener holes when

- The membrane tensile strain was 60% of the maximum tensile strain
- The maximum tensile strain was equal to the measured failure strain from tensile coupon tests of steel

It is considered that the above strain criterion is applicable to crest-fixed steel claddings made of other steel grades and thicknesses. Past research on crest-fixed steel claddings made of low grade, ductile steels showed that transverse splitting caused pull-through failures did not occur (Tang, 1998). Instead a local dimpling failure occurred. This is because of the failure strain of these ductile steels from tensile coupon tests is very high (>0.25 compared with 0.02 for G550 steel sheets) and hence the second criterion above will never be reached. This also supports the above strain criterion developed in this investigation. In this experimental study, transverse splitting caused pull-through failures occurred at a lower load for non-standard Type A profiled sheets made in the transverse direction (see Table 1). This occurred due to the reduced tensile coupon failure strain of 0.008 for G550 steel sheets in the transverse direction and hence further

confirms the reliability of the proposed strain criterion. The proposed strain criterion has been successfully used in the finite element analysis of trapezoidal claddings by Mahaarachchi and Mahendran (2004) to predict the observed transverse splitting.

4. CONCLUSIONS

This paper has presented the details of an experimental investigation into the pull-through failure mechanism of crest-fixed thin high strength steel roof claddings commonly used in Australia. The results from a large number of full-scale air-box tests and small scale tests on trapezoidal sheeting have been used to develop a strain criterion in terms of the flexural and membrane strain components at the critical central support fastener holes for the transverse splitting observed in the pull-through failures. This strain criterion can be used in the numerical modelling of these steel cladding systems. The paper also discusses the nonlinear behaviour of roofing assemblies under wind uplift pressures. It was found that the critical central support fastener loads used in design could not be predicted by conventional simple engineering formulae (Equations 3 and 4) unless appropriate modifications are made to the coefficients in these formulae. The current design formula was unconservative in predicting the pull-through failure loads of crest-fixed steel claddings.

5. ACKNOWLEGEMENTS

The authors wish to thank the Faculty of Built Environment and Engineering at Queensland University of Technology for providing the required facilities and technical support for this research project.

6. REFERENCES

Atkins, A.G. and Mai, Y.W. (1985). Elastic and Plastic Fracture, Ellis Horwood/John Wiley, Chichester.

Atkins, A.G. and Mai, Y.W. (1987). Fracture Strains in Sheet Metal Forming and Specific Essential Work of Fracture, Engineering Fracture Mechanics, 27 (3), 291-297.

Beck, V.R. and Stevens, L.K. (1979) Wind Loading Failures of Corrugated Roof Cladding, Civil Eng. Trans., IEAust; 21(1): 45-56.

Datsko, J. (1966). Material Properties and Manufacturing Processes. Wiley, New York.

Ghosh, S.K. and Travis, F.W. (1979). An Investigation into the Static and Dynamic Piercing of Diaphragms, Journal of Mech. Sci., 22, 1-22.

Mahaarachchi, D. and Mahendran, M. (2004) Finite Element Analysis and Design of Crest-fixed Trapezoidal Steel Claddings with Wide Pans subject to Pull-through Failures, Eng. Struct.; 26 (11): 1547-1559

Mahendran, M. (1990a) Fatigue Behaviour of Corrugated Roofing Under Cyclic Wind Loading, Civil Eng Trans., IEAust; 32(4): 219-226.

Mahendran, M. (1990b) Static Behaviour of Corrugated Roofing under Simulated Wind Loading, Civil Eng Trans, IEAust; 32(4): 211-218.

Mahendran, M. (1994) Behaviour and Design of Crest Fixed Profiled Steel Roof Claddings Under High Wind Forces, Eng Struct; 16(5): 368-376.

Mahendran, M. and Tang, R.B. (1999) Pull-through Strength of High Tensile Steel Cladding Systems, Australian Journal of Struct. Eng; 2(1): 37-49.

Marciniak, Z. and Kuczynski, K. (1967) Limit Strains in the Process of Stretch forming Sheet Metal. International Journal of Mechanical Science, 9, 609-620.

Muscat-Fenech, C.M. and Atkins, A.G. (1998). Denting and Fracture of Sheet Steel by Blunt and Sharp Obstacles in Glancing Collisions, Int. J. Impact Engineering, 21 (7), 499-519.

Standards Australia (SA) (1992) AS4040-2 Method of Testing Sheet Roof and Wall Cladding, Sydney, Australia.

Standards Australia (SA) (2005) AS/NZS 4600 Cold-formed Steel Structures Code, Sydney, Australia.

Tang, R.B. (1998) Local Failures of Steel Cladding Systems Under Wind Uplift, ME Thesis, Queensland University of Technology, Brisbane, Australia.

Xu, Y.L. and Reardon, G.F. (1993) Test of Screw Fastened Profiled Roofing Sheets Subject to Simulated Wind Uplift, Eng. Struct; 15(6): 423-430.

Xu, Y.L. and Teng, J.G. (1994). Local Plastic Failures of Light Gauge Steel Roofing Sheets: Finite Element Analysis versus Experiment, Journal of Construct. Steel Research, 30, 125-150.

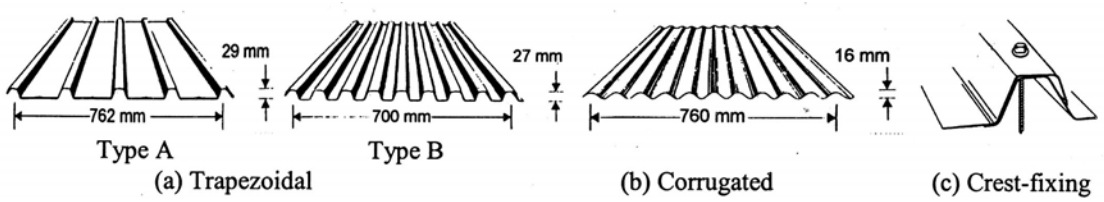

p = 190, d =29, bmt = 0.42,0.48 (Type A) p = 76, d =16, bmt = 0.42,0.48
p = 87, d =24, bmt = 0.42,0.48 (Type B)
(p = pitch in mm, d = depth in mm, bmt = base metal thickness in mm)

Figure 1. Standard Profiled Steel Cladding Systems used in Australia

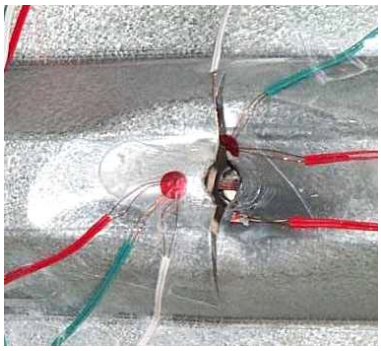

(a) Local Pull-through Failures with Transverse Splitting

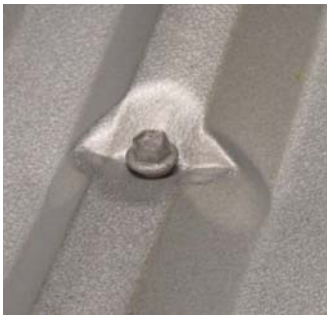

(b) Local Dimpling Failure in Type B Trapezoidal and Corrugated Roof Sheeting

Figure 2. Local Failures at Screwed Connections

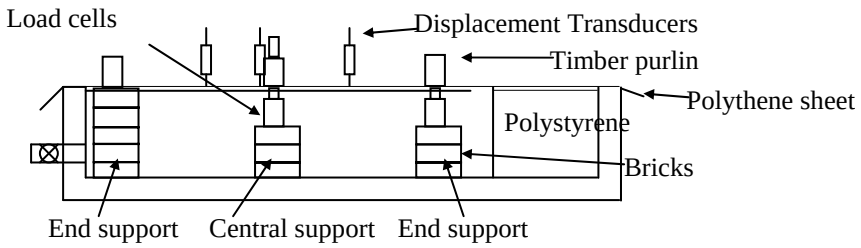

(a) Schematic Diagram

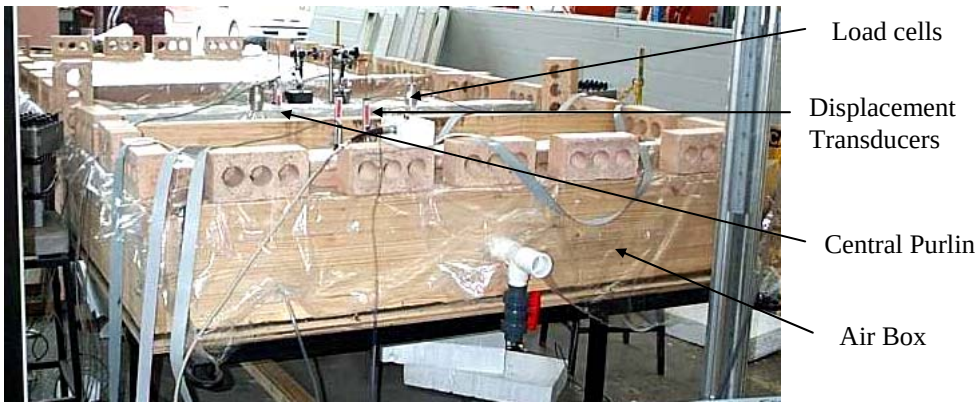

(b) Photograph showing the Air box

(c) Two-span trapezoidal Type A sheeting with 425 mm span

Figure 3. Experimental Set-up

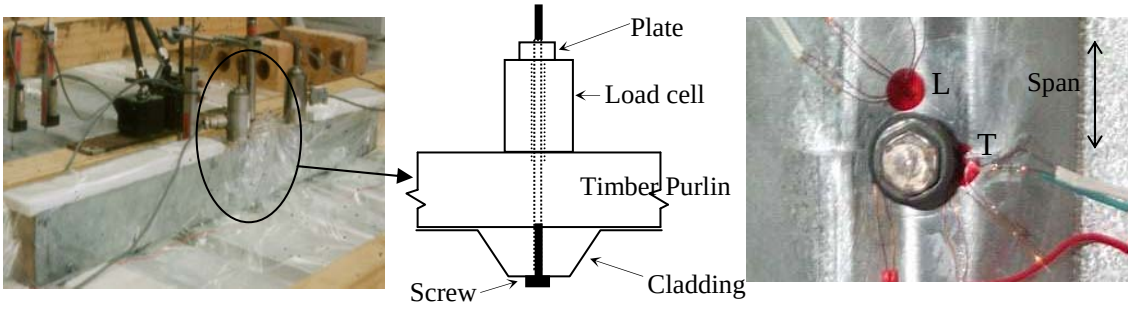

L, T = Longitudinal & Transverse sides

Figure 4. Load Cell and Strain Gauge Arrangement

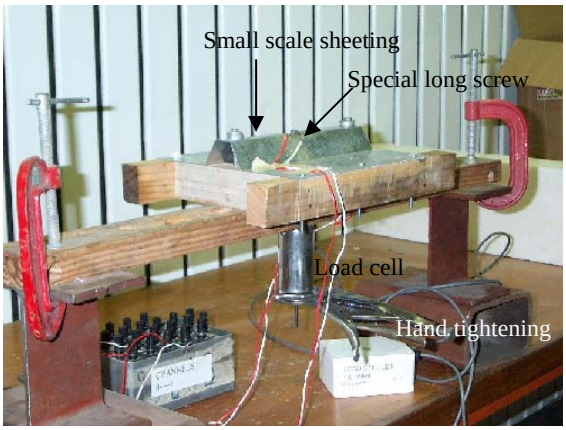

Figure 5. Small Scale Test Set-up

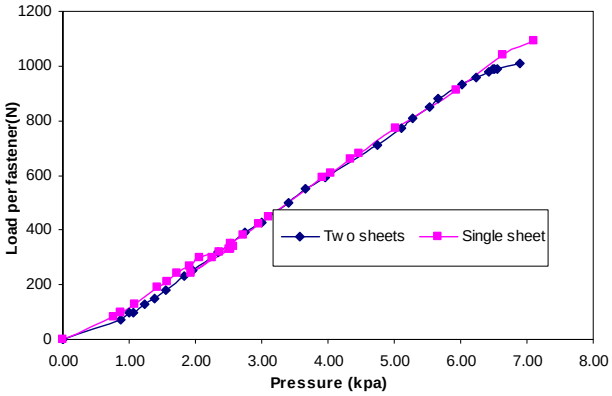

Figure 6. Comparison of Results for Single and Two Sheet Wide Specimens

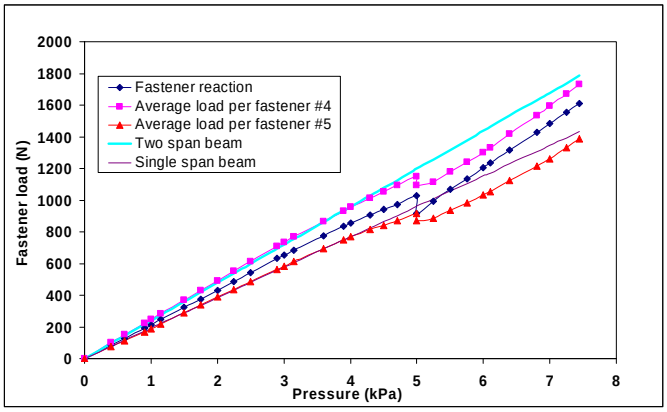

(a) Trapezoidal Type B roofing

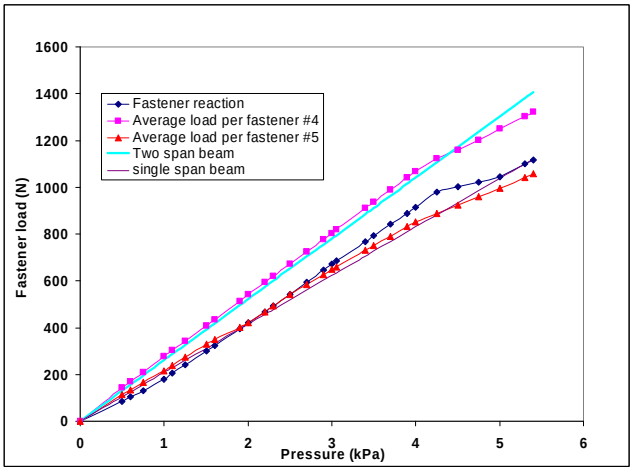

(b) Trapezoidal Type A roofing

Figure 7. Load per Fastener versus Uplift Pressure Curves

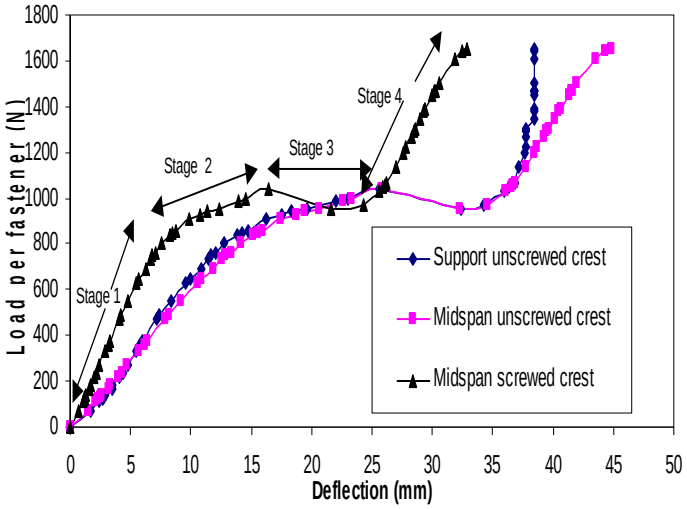

Figure 8. Load-Deflection Behaviour of Trapezoidal Type B Roofing

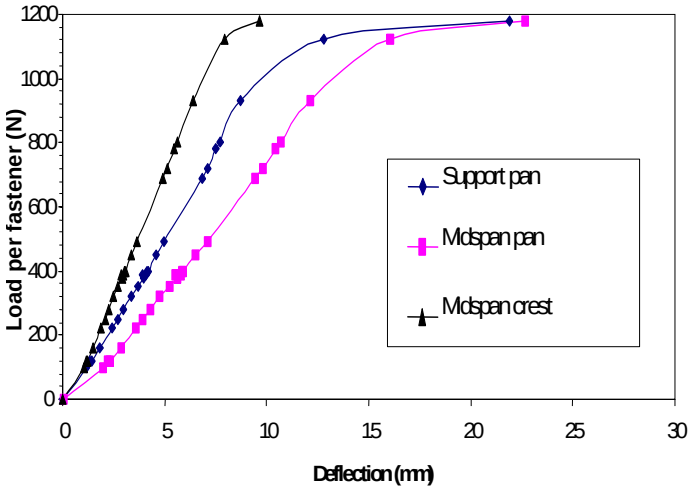

Figure 9. Load-Deflection Behaviour of Trapezoidal Type A Roofing

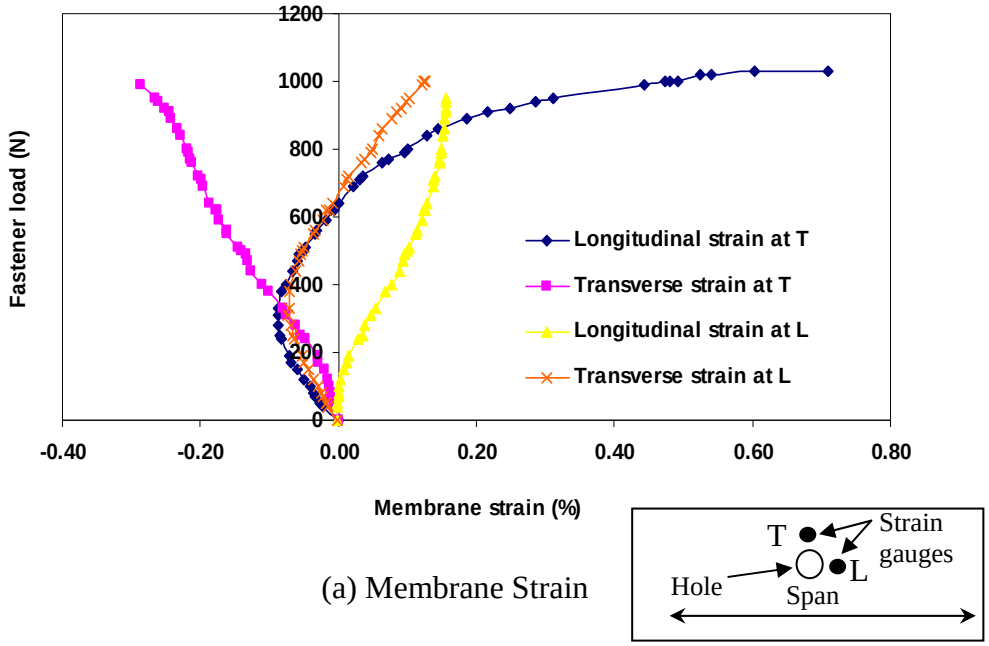

(a) Membrane Strain

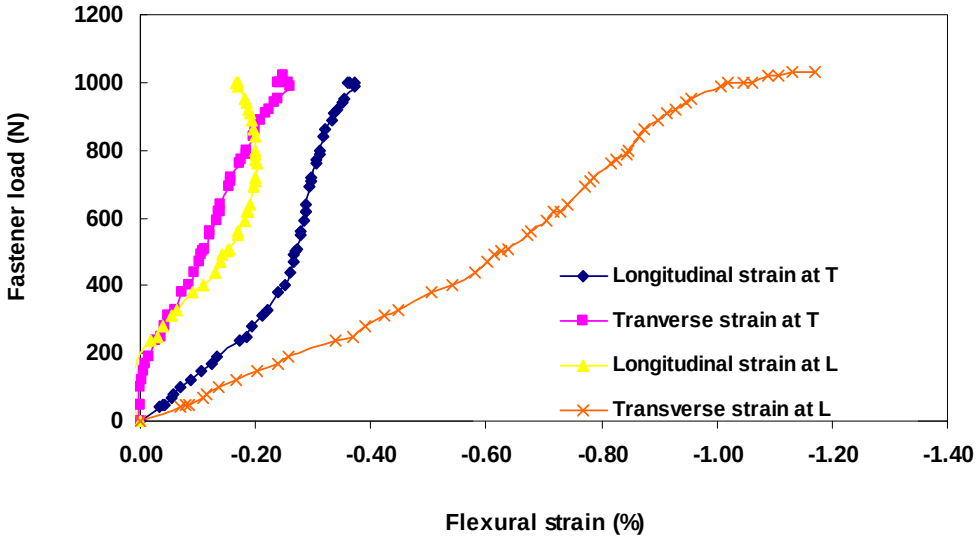

(b) Flexural Strain

Figure 10. Variations of Strains for Trapezoidal Type A Cladding

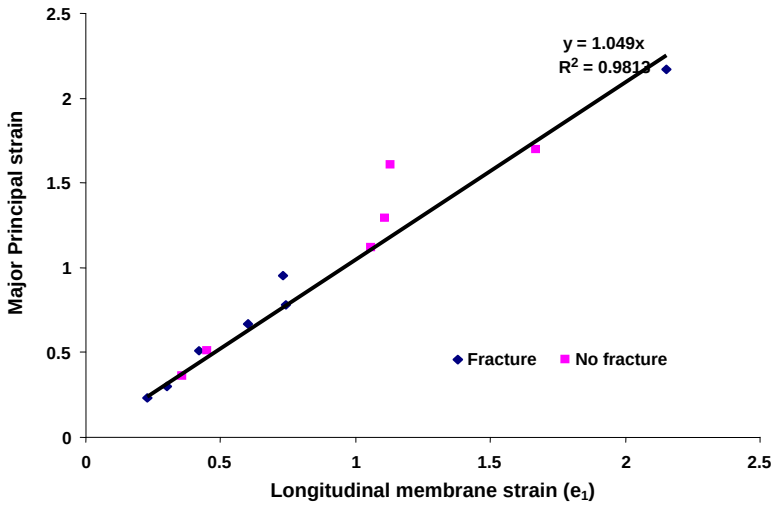

(a) Major principal strain variation with Longitudinal strain

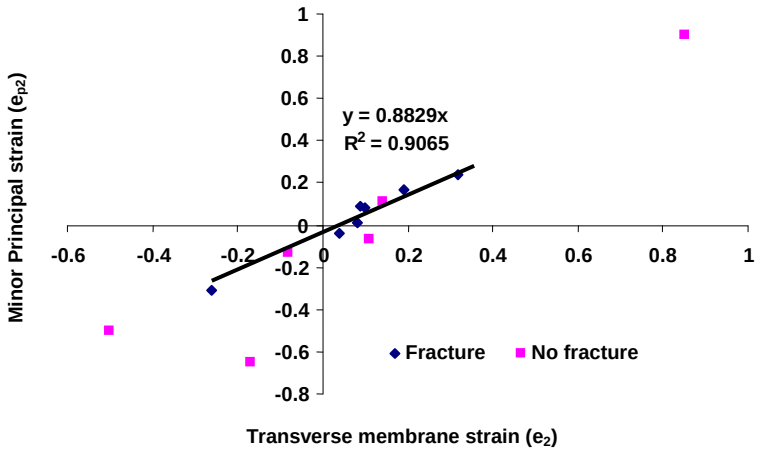

(b) Minor principal strain variation with Transverse strain

Figure 11. Relationship between Principal Strains and Membrane Strains on the Transverse Side of Fastener Hole

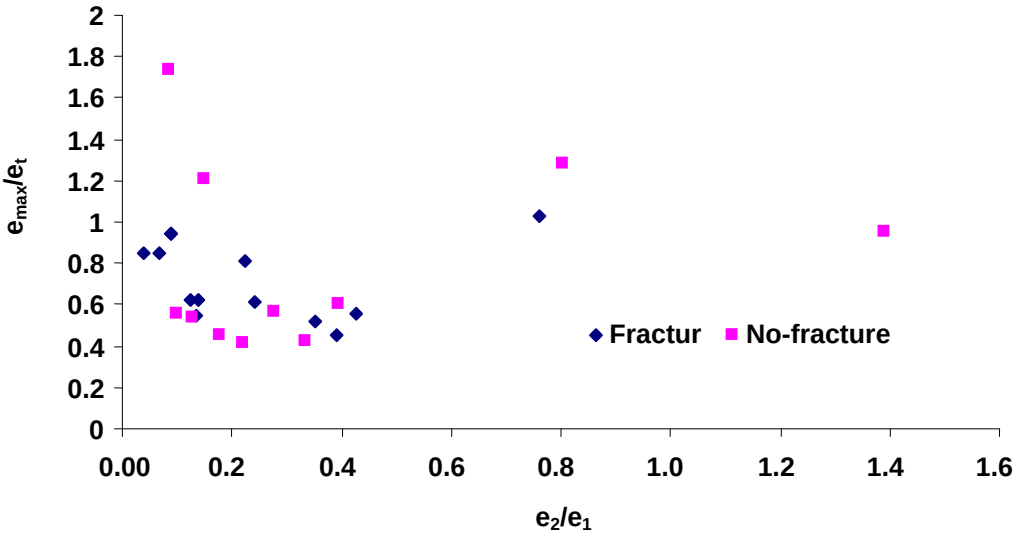

Figure 12. Maximum Surface Tensile Strain at Failure/Tensile Coupon Failure Strain (e_{max}/e_t) versus Transverse Membrane Strain/Longitudinal Membrane Strain (e_2/e_1)

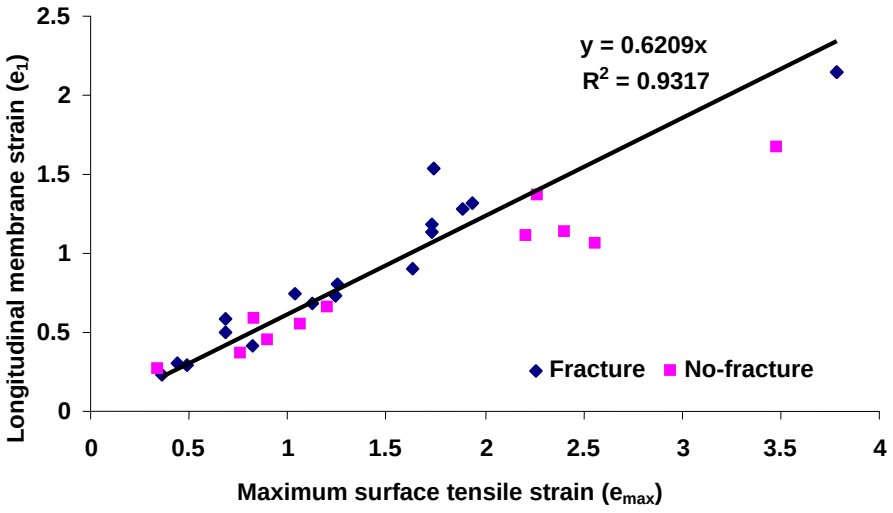

Figure 13. Relationship between Longitudinal Membrane Strain and Maximum Surface Tensile Strain on the Transverse Side of Fastener Hole at Failure

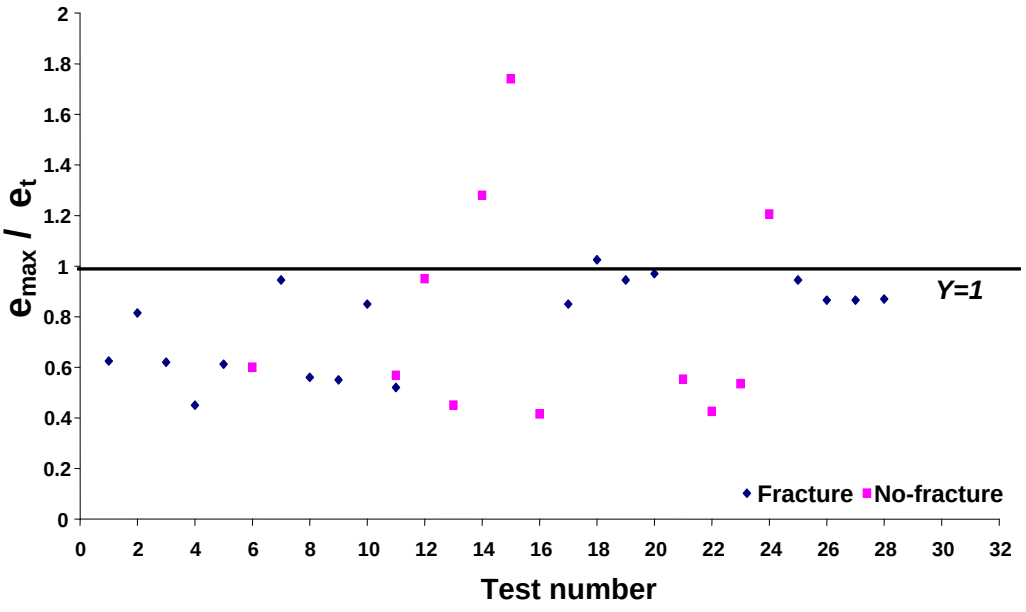

Figure 14. Maximum Surface Tensile Strain at Failure/Tensile Coupon Failure Strain (e_{max}/e_t) for Each Test (Test Number)

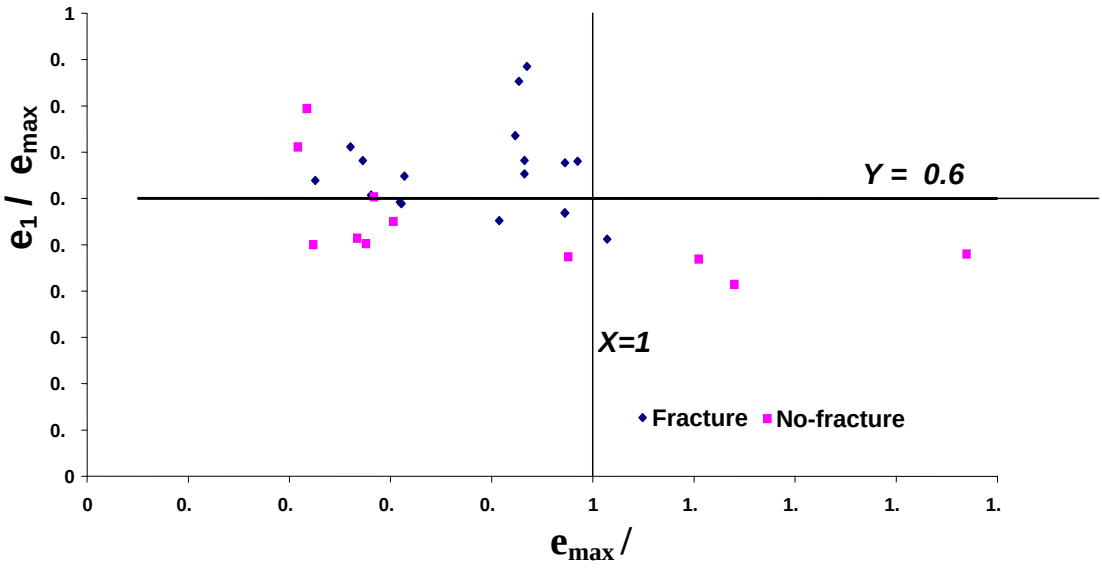

Figure 15. Plot of Longitudinal Membrane Strain/Maximum Surface Tensile Strain versus Maximum Surface Tensile Strain/Failure Strain in Tensile Coupon Test

Table 1. Fastener Failure Loads

Test Cladding and Span (mm)	Experiment (N)			Simple Equations (N)		Design Equations (N)	
	Actual	Average		Eq.3	Eq.4	Eq.1	Eq.2
		4**	5**				
Type A 900 mm	1180 1010	1372 1340	1092 1170	1418 1657	1135 1357	3248 3248	1186 1186
Type A 19 mm washers 900mm	1350	1340	1070	1446	1157	3248	1322
Type A 1000mm	1030 1070	1240 1337	992 1070	1285 1511	1028 1209	3248 3248	1186 1186
Type A 1050 mm	1070	1273	1018	1348	1078	3248	1186
Type A 1100 mm	1100	1258	978	1385	1078	3248	1186
0.48 mm Type A 900	1450	1643	1314	1054	831	3712	1590
* Type A 20 mm crest width - 425mm	800	1135	908	1184	947	3248	1186
* Type A 26 mm crest width - 425mm	730	1463	1170	1471	1177	3248	1186
* Type A 175 mm pitch - 425mm	700	1118	894	1009	807	3248	1186
* Type A 210 mm pitch - 425 mm	710	1175	940	734	587	3248	1186
* Type A 60 mm trough width-425mm	770	1170	936	1300	1040	3248	1186
Type B-900 mm	1063	1225	980	1459	1166	3248	1121
Type B-1100mm	1040	1143	914	1197	957	3248	1121
0.48 mm Type B 900	1300	1543	1234	1538	1230	3712	1406

**4 = Central support reaction /4 **5 = Central support reaction /5

* Non-standard profiles which were made in the transverse direction

Table 2. Comparison of Failure Strains on the Transverse Side of Fastener Hole

Test Cladding Type and Span in mm	Membrane Strain%		Flexural Strain %		Max. Strain	Split
	Longl.	Transv.	Longl.	Transv.		
Type A 900 mm	0.81	0.1	0.44	0.54	1.25	Yes
Type A with 19mm washers 900 mm	0.45	-0.08	0.44	0.08	0.90	No
Type A 1000 mm	0.74	-0.26	0.30	0.23	1.04	Yes
	0.90	0.20	0.80	0.40	1.63	Yes
Type A 1050 mm	0.73	0.10	0.51	0.43	1.24	Yes
	0.68	0.29	0.45	0.32	1.12	Yes
Type A 1100 mm	0.66	0.26	0.55	0.84	1.20	No
	1.06	0.85	1.50	0.61	2.56	No
0.48 mm Type A 900 mm	2.15	0.19	1.63	1.46	3.78	Yes
* Type A w_c=20mm - 425	0.30	0.04	0.14	0.25	0.44	Yes
* Type A h_c=26mm - 425	0.58	-0.04	0.1	0.22	0.68	Yes
* Type A with p=175mm	0.50	0.02	0.18	0.52	0.68	Yes
– 425 mm span	0.23	0.09	0.13	0.24	0.36	Yes
* Type A with p=210 mm	0.36	-0.50	0.40	0.46	0.76	No
– 425 mm span	0.27	0.09	0.08	0.69	0.34	No
* Type A with w_t=60mm	0.29	0.07	0.20	0.16	0.49	Yes
– 425 mm span	0.42	0.32	0.40	0.85	0.82	Yes
Type B 900 mm	1.67	0.14	1.81	0.58	3.48	No
	0.55	-0.07	0.52	0.70	1.07	No
Type B 1100 mm	1.13	-0.17	1.29	0.45	2.41	No
	0.59	0.13	0.25	0.85	0.83	No
0.48 mm Type B 900 mm	1.11	0.11	1.09	0.2	2.21	No
	1.37	0.38	0.90	1.46	2.27	No
Small Scale (SS) Type A	1.32	-	0.62	-	1.94	Yes
SS Type A w_c=20 mm	1.28	-	0.60	-	1.89	Yes
SS Type A with h_c=26mm	1.18	-	0.55	-	1.73	Yes
SS Type A with h_c=32mm	1.13	-	0.60	-	1.73	Yes
SS Type A p=175mm	1.54	-	0.20	-	1.74	Yes
SS Type A p=210 mm	2.8	-	1.42	-	4.22	Yes
SS 0.48mm TypeA w_t=60	0.59	0.07	0.34	0.17	0.93	Yes
*SS Type A	0.66	-	0.17	-	0.83	Yes
SS Type B	1.50	-	0.27	-	1.77	Yes
SS 0.48mm Type B	2.66	-	2.39	-	5.05	Yes

*Non-standard profiles which were made in the transverse direction

SS – Small scale, w_c=Crest width h_c= Crest height w_t=Trough width, p = Pitch